Mott transition of the excitons in GaSe

L. Pavesi* and J. L. Staehli
Institut de Physique Appliquée, Ecole Polytechnique Fédérale, PH-Ecublens, CH-1015 Lausanne, Switzerland

V. Capozzi
Institut de Physique Appliquée, Ecole Polytechnique Fédérale, PH-Ecublens, CH-1015 Lausanne, Switzerland and Dipartimento di Fisica, Università di Bari, via Amendola 173, I-70126 Bari, Italy

(Received 15 March 1988; revised manuscript received 17 November 1988)

An optical study of the excitonic Mott transition in GaSe at liquid-He temperature is presented. In recording the optical spectra, care was taken to reduce the effects of the spatial inhomogeneity of the photoexcited carriers as much as possible. The transition we observed is smooth and continuous. We discuss the contribution of bound and dissociated electron-hole pairs to the screening of the carrier-carrier interaction. The observed red shift of the excitonic level with increasing carrier density agrees well with the prediction of our model, which is based on a simplified binary-collision approximation.

I. INTRODUCTION

In semiconductors, photogenerated electron-hole (e-h) pairs rapidly thermalize and relax into levels close to the band gap. Direct e-h pairs normally have a short recombination lifetime which, at low crystal lattice temperatures T_l, does not allow them to thermalize with the crystal lattice. Thus, the temperature T_e of the e-h pairs is usually higher than T_l. Therefore, they will not only occupy bound states (excitons) which have the lowest energies but also higher dissociated states (ionized excitons). The relative concentration of excitons and dissociated pairs can be calculated using an appropriate mass action law.[1] The e-h pair density can be easily raised increasing the intensity of photoexcitation. A high e-h pair density will screen the Coulomb interaction between electrons and holes. For very strong screening no bound e-h pair states exist.[2,3] Thus, at low temperatures and with increasing pair density, the e-h fluid turns from an insulating gas of mostly bound e-h pairs or excitons into a metallic plasma of dissociated pairs. This phase transition is called Mott transition (MT) of the excitons,[3] even though the carriers are not at zero temperature.

We studied the Mott transition in GaSe by analyzing the recombination luminescence and transmission spectra at different excitation intensities J. In the luminescence spectra, for low J, one observes a pronounced peak at 2.110 eV caused by the recombination of the fundamental direct exciton (ex). At low J, the indirect recombinations with electrons from the conduction-band minimum at the M point of the Brillouin zone (which is some 25 meV lower in energy than the minimum at Γ) are very weak. In GaSe, the ex peak is relatively narrow and often also some excited exciton states are well resolved. Thus, GaSe is quite adequate for an optical study of the excitonic spectra. With increasing pump intensity, a low-energy shoulder appears on the ex line. At still higher J, a second peak, which is attributed to excitonic recombination assisted by an exciton-electron (ex-e) scattering process,[4,5] shows up at about 2.106 eV (see Figs. 6 and 7). With increasing J, the ex-e emission rapidly grows while the exciton emission increases at a modest rate. Both lines slowly shift to the red and become wider. Eventually, as the pump intensity is further raised, the ex-e peak is gradually replaced by the wide and smooth emission of the e-h plasma which contains Γ electrons, M electrons, and Γ holes.[6] However, a high-energy shoulder on the plasma emission persists up to e-h pair densities which are higher than the density at which the Mott transition occurs. We attribute this shoulder to the enhancement in the e-h recombination probability—the so-called excitonic enhancement[7–9]—caused by the attractive e-h interaction in the plasma.

We discuss our observations in the framework of the first-order theory developed by Stolz and Zimmermann[10] and by Röpke *et al.*[11] We evaluate self-consistently ionization ratio and binding energy of the fundamental exciton versus total e-h pair density. Further, we analyze the effects of different ways of evaluating the screening of the e-h Coulomb interaction on the optical spectra. For simplicity, we treat screening as if it were caused by direct pairs only. The contribution to screening of the indirect e-h pairs (which are present at least at high carrier densities[5,6]) does not change the qualitative features of the optical spectra.

II. THEORY

We consider an ensemble of photoexcited electrons (e) and holes (h) in an intrinsic direct-gap semiconductor. We suppose that the carriers are in a steady state characterized by an effective temperature T_e. The particles interact through a statically screened Coulomb potential. Further, we discuss our ensemble in binary collision approximation,[12,10] and beyond this we neglect e-e and h-h interactions (which are less important as long as

$k_B T_e \ll E_B$, where E_B is the unperturbed Rydberg and k_B is the Boltzmann constant[10]) and keep the e-h interaction only. Making these approximations we can separate the center-of-mass motion from the relative motion of the e-h pairs. The center-of-mass motion is not affected by the interactions. An increase of the e-h pair density causes an increase of the screening of the e-h interaction, which in turn induces a lowering of the exciton binding energy. For a strong enough screening, bound states cease to exist and the e-h pair system is formed by dissociated e-h pairs only.[2,3] While the bound e-h pairs contribute to the dipolar screening the dissociated excitons cause metallic screening. In static screening approximation, the e-h interaction can be described by a Yukawa potential (YP) (Ref. 1):

$$V_{eh}(r) = -\frac{q^2}{\epsilon_{\rm ex}} \frac{\exp(-r/r_{\rm sc})}{r} , \tag{1}$$

where r is the distance between the particles in a pair and q is the electronic charge. The exponential screening with a characteristic length

$$r_{\rm sc} = \left[\frac{\epsilon_{\rm ex}}{4\pi q^2} \left[\frac{dn_f}{d\mu_e} + \frac{dn_f}{d\mu_h} \right]^{-1} \right]^{1/2} \tag{2}$$

is caused by the free electron-hole pairs of density n_f and chemical potential $\mu_e + \mu_h$. In nondegenerate limit,

$$r_{\rm sc} = \left[\frac{\epsilon_{\rm ex}}{8\pi q^2} \frac{k_B T_e}{n_f} \right]^{1/2} , \tag{3}$$

which does not depend on the carrier masses.

The static dielectric constant $\epsilon_{\rm ex}$ also contains the contribution of the bound e-h pairs of density $n_{\rm ex}$. Experimental data show that the screening caused by paired excitons is much weaker than the screening caused by dissociated e-h pairs;[13] we therefore replaced in Eq. (1) $\epsilon_{\rm ex}$ by the static dielectric constant of the unperturbed crystal ϵ_0.

The numerical solution of the radial Schrödinger equation for the relative motion of an e-h pair interacting through a YP has been studied in Refs. 2 and 8. The fundamental exciton state disappears at a critical screening length called Mott value:

$$r_{\rm sc}^M = 0.8399 a_B , \tag{4}$$

(where a_B is the Bohr radius of the unperturbed exciton). For $r_{\rm sc} < r_{\rm sc}^M$ no bound states exist.

A. Density of states and partition function

We first consider the energy spectra. Since interpair interactions are not included in our approximation, the density of states (DOS) of the center-of-mass motion of the e-h pairs is that of an ideal gas. For the DOS of the relative motion, we can write[8]

$$D_r^{(eh)}(E_r) = D_r^0(E_r) + \Delta D_r^{(eh)}(E_r) , \tag{5}$$

where

$$D_r^0(E_r) = 2 \frac{(2m_{eh})^{3/2}}{4\pi^2 \hbar^3} (E_r)^{1/2} \tag{6}$$

is the density of states at energy E_r if the particles were not interacting (m_{eh} is the reduced mass of the e-h pair). $\Delta E_r^{(eh)}$ is a correction due to the presence of the e-h interaction:[14]

$$\Delta D_r^{(eh)}(E_r) = \frac{1}{v} \sum_l (2l+1) \left[\sum_n \delta(E_{n,l}^{(eh)} - E_r) + \frac{1}{\pi} \frac{d\eta_l(E_r)}{dE_r} \Theta(E_r) \right] . \tag{7}$$

Here, $E_{n,l}^{(eh)} < 0$ is the energy of a bound e-h pair state with angular momentum $\hbar l$, $\eta_l(E_r)$ is the phase shift caused by the interaction in the radial wave function $R_l(r, E_r)$ at large interparticle distance of a continuum state (having the same angular momentum $\hbar l$) with energy $E_r > 0$, the subscript r indicates that the relative motion is considered, and $\delta(E)$ and $\Theta(E)$ are the common δ and unit step functions.

We consider now the whole gas of e-h pairs characterized by its total density n_t, its temperature T_e, and its chemical potential μ. In analogy to Eq. (5), we can write[8,10]

$$n_t = n^0 + \Delta n^{(eh)} , \tag{8}$$

where n^0 is the density without interactions, i.e.,

$$n^0 = 2 \left[\frac{m_{eh} k_B T_e}{2\pi\hbar^2} \right]^{3/2} \exp\left[\frac{\mu_r}{k_B T_e} \right] \tag{9}$$

and $\Delta n^{(eh)}$ is a correction caused by the intrapair interactions. In quasiclassical limit,

$$\begin{aligned} \Delta n^{(eh)} &= \exp\left[\frac{\mu_c + \mu_r}{k_B T_e} \right] \int D_c^0(E_c) \exp\left[-\frac{E_c}{k_B T_e} \right] \times dE_c \Delta Z_r^{(eh)} \\ &= (n^0)^2 \frac{1}{2} \left[\frac{2\pi\hbar^2}{m_{eh} k_B T_e} \right]^{3/2} \Delta Z_r^{(eh)} , \end{aligned} \tag{10}$$

where the subscript c refers to the motion of the center-of-mass, and

$$\Delta Z_r^{(eh)} = v \int \Delta D_r^{(eh)}(E_r) \exp\left[-\frac{E_r}{k_B T_e} \right] dE_r \tag{11}$$

is the interaction part of the partition function which contains the contributions Z_b and $\Delta Z_{rf}^{(eh)}$ of bound and scattering states.

Stolz and Zimmermann[10] discuss the partition function (11). They factorize the Fourier transform of the screened Coulomb potential (1) in order to obtain analytical formulas. In particular, from their results it follows that the effect of e-e interactions is smaller than the effect of e-h interactions, i.e.,

$$|\Delta Z_r^{(eh)}| > |\Delta Z_r^{(ee)}| , \tag{12}$$

which justifies our above-mentioned neglectance of the e-e (and h-h) interactions.

The numerical solution of the radial part of the Schrödinger equation of the e-h pair for a given screening length r_{sc} (Ref. 8),

$$-\frac{\hbar^2}{2m_{eh}r^2}\left[\frac{d}{dr}\left[r^2\frac{dR_l}{dr}-l(l+1)\right]\right] -\frac{e^2}{\epsilon_0 r}\exp\left[-\frac{r}{r_{sc}}\right]R_l=E_rR_l\ , \quad (13)$$

through Eq. (7) gives $\Delta D_r^{(eh)},(E_r,r_{sc})$ from which we calculated $\Delta Z_r^{(eh)}(r_{sc})$.

The results, given in Fig. 1, are qualitatively similar to those obtained using the analytical method of Ref. 10. Looking at Fig. 1, we see that the contribution of the bound states, Z_b, decreases with r_{sc}, due to the lowering of the binding energy. At r_{sc}^M, Z_b goes discontinuously from one to zero as a consequence of the disappearance of all bound states. On the other hand, $\Delta Z_{rf}^{(eh)}$, which represents the effects of the e-h interaction in the continuum, changes sign at the Mott transition. For $r_{sc}\geq r_{sc}^M$, $\Delta Z_{rf}^{(eh)}$ is negative, because each time a bound state is approaching the continuum the correction $\Delta D_r^{(eh)}$ $(E_r\geq 0)$ to the DOS is negative.[8] For $r_{sc}<r_{sc}^M$, also the lowest $(1s)$ bound state has joined the continuum; however, it *survives* as a peak in the DOS at the bottom of the continuum. Such a peak is called a zero-energy state or quasiresonance by nuclear theorists.[15] Its positive contribution to $\Delta Z_{rf}^{(eh)}$ replaces Z_b and consequently $\Delta Z_r^{(eh)}$ is always continuous. This explains the continuity of the thermodynamic and optical properties of the e-h fluid at the Mott transition. Finally, an increase of the carrier temperature reduces the variation in $\Delta Z_r^{(eh)}$ with r_{sc} because the low-energy states (which are mostly affected by the e-h interaction) have a reduced population and thus their relative contribution to $\Delta Z_r^{(eh)}$ is reduced.

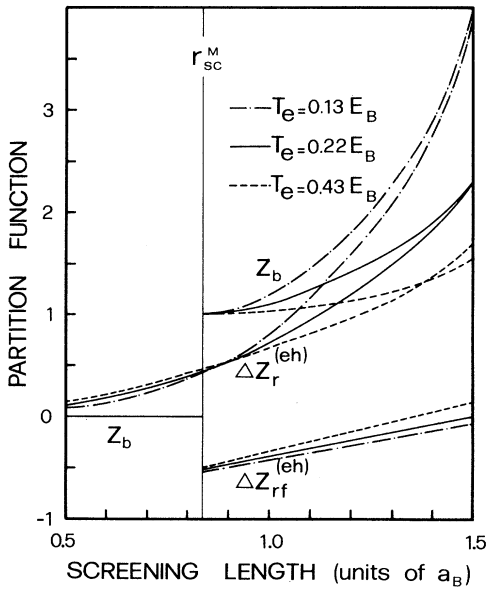

FIG. 1. Interaction part $\Delta Z_r^{(eh)}=Z_b+\Delta Z_{rf}^{(eh)}$ of the partition function for the relative motion of an electron-hole pair interacting via a screened Coulomb potential [Eq. (1)], vs screening length r_{sc}. The contributions Z_b and $\Delta Z_{rf}^{(eh)}$ of the bound and scattering states, respectively, have been calculated using Eq. (11) for three temperatures. In GaSe, these temperatures correspond to 30, 50, and 100 K. At $r_{sc}=r_{sc}^M\simeq 0.84a_B$ the Mott transition of the excitonic ground state occurs (Ref. 2).

B. Ionization ratio and screening

The total e-h pair density as given by Eq. (8) can be divided in different ways. Obviously the exciton density

$$n_{ex}=(n^0)^2\frac{1}{2}\left[\frac{2\pi\hbar^2}{m_{eh}k_BT_e}\right]^{3/2}Z_b \quad (14)$$

is a part of the correction $\Delta n^{(eh)}$ caused by the e-h interactions

$$\Delta n^{(eh)}=n_{ex}+\Delta n_f^{(eh)}\ , \quad (15)$$

where

$$\Delta n_f^{(eh)}=(n^0)^2\frac{1}{2}\left[\frac{2\pi\hbar^2}{m_{eh}k_BT_e}\right]^{3/2}\Delta Z_{fr}^{(eh)} \quad (16)$$

is the correction for the dissociated pair density

$$n_f=n^0+\Delta n_f^{(eh)}\ . \quad (17)$$

The ionization ratio ξ is given by

$$\xi\equiv\frac{n_f}{n_{ex}+n_f}\ . \quad (18)$$

The correlation degree γ, introduced in Ref. 12, is a measure of the importance of the e-h interactions in the carrier gas:

$$\gamma=\frac{n_{ex}+\Delta n_f^{(eh)}}{n_{ex}+n_f}\ . \quad (19)$$

It is different from zero at densities above the Mott value, too. From optical experiments, however, it is normally easier to determine the ionization ratio ξ.

In ionization equilibrium, n_{ex} and n_f are related to each other by a mass action law, as given by Eqs. (14)–(17). For a consistent determination of energy levels and ionization ratio, we made use of the interaction parts $Z_b(r_{sc})$ and $\Delta Z_{rf}^{(eh)}(r_{sc})$ of the partition function calculated in Sec. II A. And as far as screening is concerned, we consider three ways of estimating r_{sc}.

(i) *Free-carrier screening.* Only the dissociated pairs of density n_f contribute to screening and r_{sc} is given by Eq. (3). The solution of the four equations (3) and (13), (14), and (17) yields the four quantities n^0, n_{ex}, n_f, and Δn_f. Plots of these quantities are shown in Fig. 2. A problem arises with this model, as can be seen from Fig. 3: $n_t(r_{sc})$ is discontinuous at the Mott transition [for r_{sc} slightly longer than r_{sc}^M, there is even no real solution of $n_t(r_{sc})$]. The excitons whose contribution to screening has been neglected become ionized and thus are suddenly contrib-

uting to metallic screening. Consequently, the e-h correlation strongly decreases once $r_{sc} < r_{sc}^{M}$ [see Figs. 2(c) and 2(d)]. We discuss two possibilities to overcome this problem.

(ii) *"Uncorrelated" screening.* As proposed in Ref. 10, in order to compute the screening length, n^0 can be used instead of n_f. This means that for the evaluation of the screening effects, the e-h correlation is neglected:

$$r_{sc}^2 \simeq r_0^2 \equiv \frac{\epsilon_0}{8\pi q^2}\frac{k_B T_e}{n^0} . \tag{20}$$

$n_t(r_0)$ is continuous also at the MT.

(iii) *Screening with exciton contribution.* The ionization of the excitons at the Mott transition is continuous. As the density of e-h pairs increases, collision broadening of the energy levels becomes more and more important. Thus the high-energy tail of the excitonic fundamental level merges with the continuum states already at pair densities below the Mott value; i.e., the contribution of the excitons to screening progressively becomes metallic. This qualitative picture is confirmed by the theoretical considerations given in Ref. 16. The e-h interaction in a dense exciton gas derived there has several contributions, all of which have the form given in Eq. (1). We use a rough but simple way to account for the contribution to screening of the excitons. For the screening length we write

$$r_{sc}^2 \simeq r_{fx}^2 \equiv \frac{\epsilon_0}{8\pi q^2}\frac{k_B T_e}{[n_f + (1 - E_b/E_B) n_{ex}]} , \tag{21}$$

where $E_b = E^{(eh)}(r_{sc})$ is the binding energy of the screened exciton. Thus in this model the excitons con-

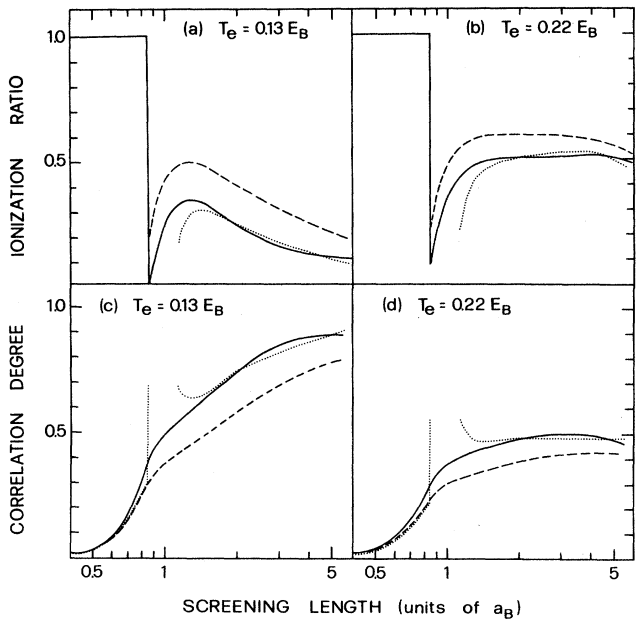

FIG. 2. Ionization ratio ξ and correlation degree γ vs screening length r_{sc}, for two carrier temperatures T_e. In GaSe, these temperatures correspond to 30 and 50 K. The curves have been calculated using different approximations to the screening length r_{sc} (see text): the dotted curves refer to the screening by free e-h pairs [Eq. (3)], the solid curves refer to the screening by "uncorrelated" pairs [Eq. (20)] (Ref. 10), and for the dashed curves a contribution of the excitons to screening has been taken into account [Eq. (21)]. In the case of free-carrier screening, there is a discontinuity at the Mott transition. To compute the curves the masses $m_{e\perp}=0.17m_0$, $m_{e\parallel}=0.3m_0$, $m_{h\perp}=0.8m_0$, and $m_{h\parallel}=0.2m_0$ (Ref. 45) have been used together with a dielectric constant $\epsilon_0=9.3$ (see also Fig. 1 of Ref. 6). The binding energy $E_B=20$ meV and the Bohr radius $a_B=3.7$ nm of the unperturbed direct exciton have been calculated taking the reciprocally averaged masses; for all other quantities the geometric ("density-of-states") mean of the masses has been used.

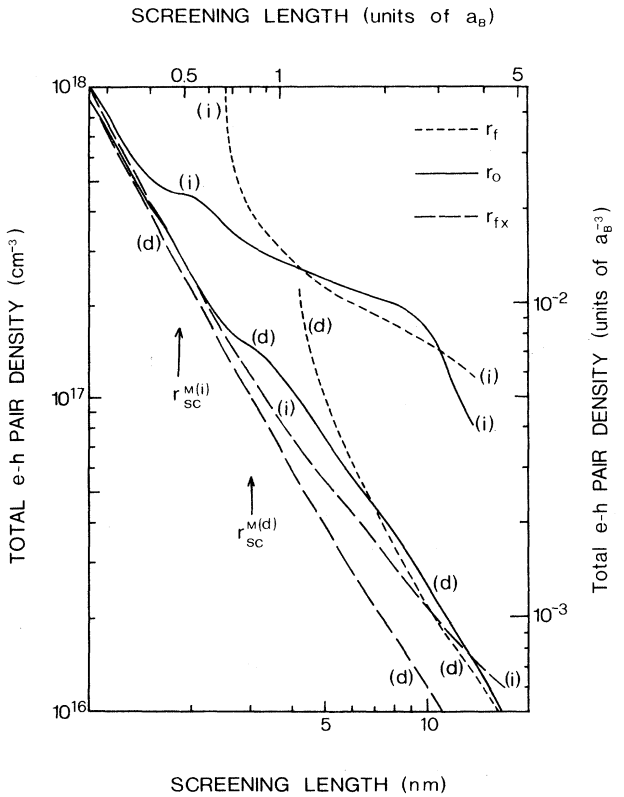

FIG. 3. Total e-h pair density n_t as a function of the screening length r_{sc} for a carrier temperature T_e which equals 40 K in GaSe. The short-dashed curves are referred to the screening by free e-h pairs [Eq. (3)], the solid curves refer to the screening by "uncorrelated" pairs [Eq. (20)] (Ref. 10), and for the long-dashed curves a contribution of the excitons to screening has been taken into account [Eq. (21)]. In the case of free-carrier screening, there is a discontinuity at the Mott transition. For $r_{sc} < r_{sc}^{M}$ the short-dashed and long-dashed curves coincide. The curves have been calculated for direct (d) and indirect (i) e-h pairs. E_B and a_B refer to the binding energy and the Bohr radius of the direct exciton. $r_{sc,M}^{d}$ and $r_{sc,M}^{i}$ indicate the critical screening length for direct and indirect excitons, respectively.

tribute in part to metallic screening; this part increases with decreasing binding energy and eventually becomes 1 at the Mott transition. $n_t(r_{fx})$ and $dn_t(r_{fx})/dr_{fx}$ (for $l=0$ states[2,8]) are continuous also at the Mott density (Fig. 3).

We note that for all three approximations discussed, the ionization ratio [Figs. 2(a) and 2(b)] has a sharp minimum at a screening length just slightly above the Mott value. This is caused by the very small exciton binding energy and the negative peak in $\Delta D_r^{(eh)}$ at the bottom of the continuum which appears when an $l=0$ bound state is about to merge with the continuum[8] (for $k_B T_e \ll E_B$, Δn_f tends to $-n^0$). However, a discussion of the ionization ratio for densities close to the Mott value is somewhat academic since for carrier densities close to the Mott value the energy levels are broadened and bound and free pairs cannot be distinguished.

The degree of correlation $\gamma(r_{sc})$ [Figs. 2(c) and 2(d)] decreases smoothly when screening becomes stronger (except in the case of free-carrier screening). At the Mott transition, γ is still appreciably different from zero; it vanishes at a screening length which is roughly half the Mott value. With increasing temperature the ionization ratio of course increases while the correlation degree becomes smaller at low carrier densities and bigger for $n_t \geq n_M$. A contribution of the free excitons to screening ($r_{sc}=r_{fx}$) increases the ionization ratio and lowers the correlation degree.

Another problem is caused by the particular structure of the conduction band in GaSe, i.e., by the presence of electrons of unknown density at the M point of the Brillouin zone. These electrons contribute to the screening, too. In Fig. 3, plots of the total e-h pair densities n_t versus screening length r_{sc} are shown. These plots are given for the two limiting cases where only direct or only indirect e-h pairs are present. We note that at the highest densities the two cases coincide because for a perfect (noninteracting) gas the screening does not depend on the carrier mass [Eq. (3)]. Further, the screening length at which the Mott transition occurs is smaller for indirect than for direct excitons because the indirect-exciton binding energy (30 meV) is larger than the direct one (20 meV). From our direct e-h pair luminescence we deduce that the screening lengths of interest for this work are $r_{sc} \geq 2.5$ nm. In this range of r_{sc} and as long as the indirect pair density is not considerably higher than the direct pairs, the effect of the M electrons is negligible for free-carrier and "uncorrelated" screening.[17] On the other hand, in the case of screening with exciton contribution, direct and indirect pairs contribute almost equally to r_{sc}; thus the total carrier density n_t is the sum of direct and indirect e-h pair densities:

$$n_t \simeq n_t^{(d)} + n_t^{(i)} . \tag{22}$$

The qualitative features in the optical spectra, however, remain unaffected since we observe only the direct optical transitions. Finally, for the purpose of comparison with the experiment, we prefer to express the computed quantities as a function of n_t rather than as a function of r_{sc}, because n_t depends directly on the excitation intensity.

C. The energy shift of the excitonic ground state

The presence of e and h at high carrier densities in a semiconductor shifts and broadens the electronic states (see, e.g., Ref. 3). The energy of the dissociated e-h pairs is reduced by an amount which does not depend on the wave vectors of the particles in their respective bands to a good approximation. As for the excitonic states, a variational calculation in a first-order Born approximation and in the framework of a screened ladder approximation has been presented in Ref. 11. This calculation, which accounts for dynamical screening effects, yields (in linear approximation) the following energy shift ΔE_{ex} of the excitonic ground state:

$$\Delta E_{ex} = \delta_{ex} n_{ex} + \delta_f^1 n_f + \delta_f^2 n_f + \delta_f^3 n_f . \tag{23}$$

δ_{ex} and $\delta_f^1, \delta_f^2, \delta_f^3$ are coefficients which depend on the carrier temperature T_e and on the effective mass ratio $\sigma = m_e/m_h$.

We have generalized the results of Ref. 11 to arbitrary carrier masses (see the Appendix). In Fig. 4, the energy-shift coefficients are shown for GaSe ($\sigma=0.4$) versus car-

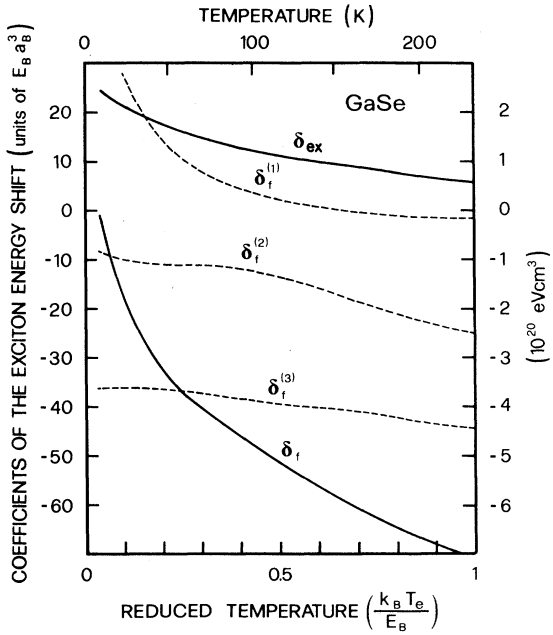

FIG. 4. Coefficients for the linear shift ΔE_{ex} of the excitonic ground-state energy for GaSe [Eq. (23) and the Appendix] vs carrier temperature T_e. The formulas derived by Röpke *et al.* (Ref. 11) for $m_e=m_h$ have been generalized to arbitrary mass ratios σ. In GaSe, $\sigma=0.4$. E_B and a_B are the binding energy and the Bohr radius of the unperturbed direct exciton. For the numerical values of the parameters, refer to the caption of Fig. 2.

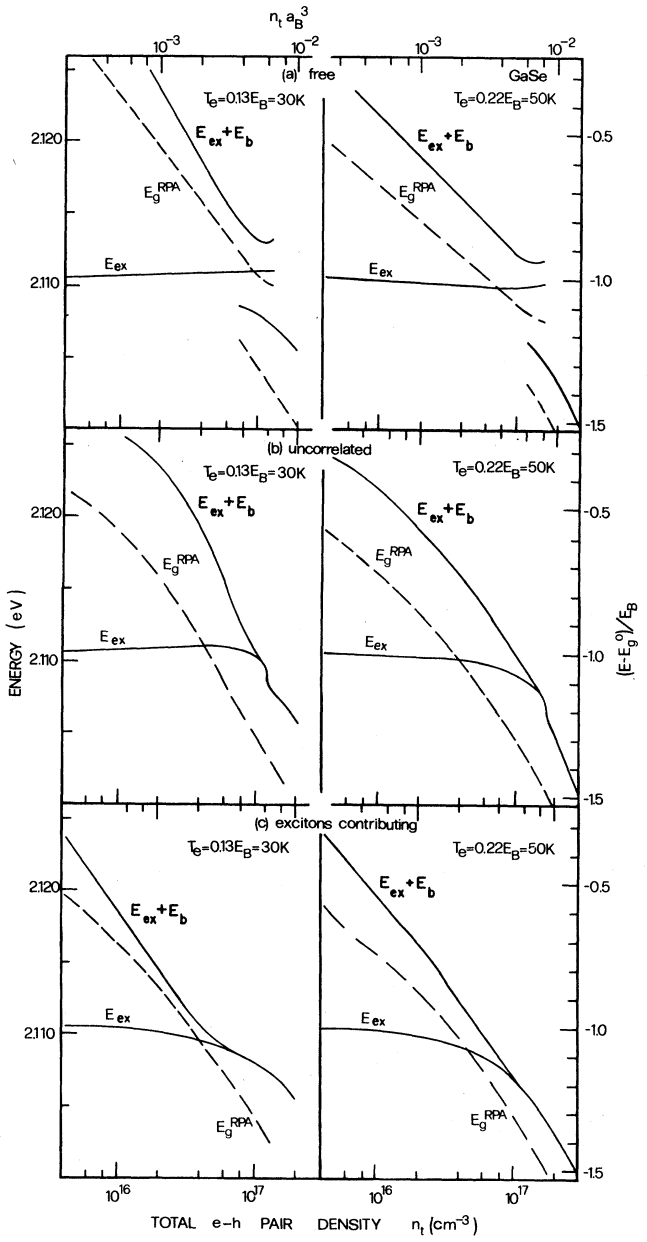

FIG. 5. Ground-state energy $E_{ex}=E_{ex}(0)+\Delta E_{ex}$ of the free exciton and width $E_g'=E_{ex}+E_b$ of the reduced energy gap vs the total e-h pair density in GaSe. $E_g^{RPA}(n_f(r_{sc}))$ is the reduced gap calculated using the analytic approximation of Thuselt (Ref. 18) (random-phase approximation in a degenerate e-h plasma). In (a), the curves have been calculated using the exciton and free e-h pair densities n_{ex} and n_f as extracted from the mass action law, Eqs. (14)–(17). For the curves in (b) [$E_g^{RPA}(n_f(n_t))$ included], n_{ex} has been replaced by $\Delta n^{(eh)}$ and n_f by n^0 [Eqs. (10) and (9), respectively (Ref. 10)]; in (c), n_{ex} has been replaced by $n_{ex}E_b/E_B$ and n_f by $n_f+(1-E_b/E_B)n_{ex}$. The numerical values of the parameters of GaSe are given in the caption of Fig. 2.

rier temperature. We note that δ_{ex}, which is due to self-energy and exchange effects of the exciton-exciton interactions, is always positive, i.e., the presence of other excitons tends to increase the exciton ground-state energy. $\delta_f \equiv \delta_f^1+\delta_f^2+\delta_f^3$, which is due to the presence of dissociated particles, is usually negative. δ_f^1 includes the band filling and the self-energy effects, δ_f^2 the plasmon-stimulated transitions from the ground state into a bound two-particle state, and δ_f^3 the transitions into scattering two-particle states.[11]

We calculated the energy shifts ΔE_{ex} in three different ways which correspond to the three approximations of the screening length discussed in the previous paragraphs. For free-carrier screening [$r_{sc}=r_f$, Eq. (3)], Eq. (23) has been used directly; in the case of "uncorrelated" screening [$r_{sc}=r_0$, Eq. (20)], Eq. (23) was replaced by

$$\Delta E_{ex}=\delta_{ex}\Delta n^{(eh)}+\delta_f n^0 \tag{24}$$

and for screening including an excitonic contribution [$r_{sc}=r_{fx}$, Eq. (21)] the shift ΔE_{ex} becomes

$$\Delta E_{ex}=\delta_{ex}\frac{E_b}{E_B}n_{ex}+\delta_f\left[n_f+\left[1-\frac{E_b}{E_B}\right]n_{ex}\right]. \tag{25}$$

Graphs of the energy $E_{ex}(n_t)=E_{ex}(n_t=0)+\Delta E_{ex}(n_t)$ of the fundamental exciton state are given in Fig. 5. For densities above the Mott value and for the nondegenerate case this energy coincides with the width E_g' of the reduced gap.[8,2] At low densities $E_g'=E_{ex}+E_b$, where the binding energy E_b of the screened exciton is known from the solution of the Schrödinger equation (13). For free-carrier screening, the Mott transition shows again a discontinuity and a hysteresis effect. In the "uncorrelated" approximation, $E_{ex}(n_t)$ and $E_g'(n_t)$ have a little kink at the Mott transition, while in the case where the excitons also contribute to screening all the curves are quite smooth. For comparison, the reduced gap $E_g^{RPA}(n_t)$, calculated using the approximation of Thuselt[18] which is valid for a degenerate e-h plasma, is also shown. E_g^{RPA} is always smaller than E_g'.

At this point let us note that for the calculation of the coefficients δ in Eq. (23) plasmon effects have been accounted for,[11] while all other considerations have been made in a simple static approximation. The full solutions of the Schrödinger equation (13) versus carrier density and temperature for an e-h interaction potential which includes plasmon effects requires important numerical work. In fact, we not only need the e-h pair binding energies but also the density of the continuum states and (as discussed below) the wave functions. On the other hand, the theory presented in Ref. 19, which partially includes plasmon effects, predicts a red shift of the exciton which is quite similar to ours.

D. Excitonic enhancement

We have previously shown using our simple model that the e-h correlations are still relevant in the plasma phase (see Fig. 2 and also Refs. 7, 8, and 9). These correlations, which are sometimes also called final-state interactions,

not only influence the density-of-pair states but also the optical interband transition probability. The excitonic enhancement factor $\rho(E_r)$ can be defined through[7,9]

$$\epsilon_2(\hbar\omega = E_g' + E_r) \equiv \rho(E_r)\epsilon_2^0(E_g' + E_r) , \quad (26)$$

where $\hbar\omega$ is the photon energy, E_r is the energy of the relative motion of the e-h pair created or destroyed by the transition, $\epsilon_2(\hbar\omega)$ is the imaginary part of the dielectric function of the real e-h gas, and $\epsilon_2^0(\hbar\omega)$ would be the same quantity of the e-h gas if the interactions were absent. Of course Eq. (26) makes sense only if no bound states are present. Normally the change $\Delta D_r^{(eh)}(E_r)$ in the DOS of the e-h pairs [Eq. (5)] caused by the interactions is negligibly small. Therefore, in a dilute e-h plasma, the excitonic enhancement factor becomes

$$\rho(E_r) = |F_{0,0}(E_r, r=0)|^2 , \quad (27)$$

where $F_{l,m}(E_r, r=0)$ is the wave function for the relative motion of an e-h pair having an angular momentum $\hbar l$ and an interparticle distance r; it is known from the solution of the Schrödinger equation (13). In the dilute limit, $\rho(E_r)$ has a peak at $E_r = 0$;[8] for degenerate e-h plasmas the peak is shifted to the chemical potential.[7,9]

III. EXPERIMENTAL METHODS

The GaSe crystals investigated have been grown by the Bridgman method ("B" samples) or by transport reaction ("T" samples). We selected them on the basis of their excitonic transmission spectrum, measured at a bath temperature of 2 K. The half-width of the ground-state exciton line was 2 meV for the T samples (the $n=3$ exciton peak could be observed) and 6 meV for the B ones. The thickness of the crystal platelets was determined optically from the interference fringes in the transmission spectra; it varied between 2 and 15 μm. Usually the c axis is perpendicular to the platelet plane. The crystals were immersed in superfluid He and pumped optically by the frequency-doubled emission at 532 nm of a YAG:Nd laser. The excitation pulses had a duration of about 120 ns and a repetition rate of 75 Hz. The illuminated spot on the sample had a diameter of about 70 μm. For the luminescence measurements, the emitted light was collected from the front surface of the sample in a direction which was an angle of $\pi/4$ inclined with respect to the c axis. A pin hole was placed in the image plane of the collecting lens, so that only the light coming from the excited volume was detected. The luminescence was analyzed by a double spectrometer and detected by a photomultiplier tube. The spectra were recorded using boxcar techniques. We also performed simultaneous transmission and reflectivity measurements using a two-beam method; details are given in Ref. 20.

The intensity J absorbed by the crystals varied between 0.002 and 2 MW cm^{-2}. The absorption coefficient of GaSe at 532 nm is about 10^3 cm^{-1}.[21] Assuming a lifetime of 0.1 ns,[22] we estimate a total e-h pair density ranging from 5×10^{14} to 5×10^{17} cm^{-3} at the surface of the sample. In our thickest samples we expect a considerable density variation with depth. However, comparing the experimental spectra from thick (10 μm) and thin (5 μm) samples, we do not observe any important difference. In particular, the observed shifts of the different peaks are, within experimental error, the same for all samples. In any case, the experimental data presented in this work were taken from samples which are about 5 μm thick. Thus the e-h pair density should not vary by more than a factor of 1.6. Since our comparison between experimental results and theoretical predictions is only semiquantitative, we consider homogeneously excited samples. Data from a thicker sample are presented in Ref. 12.

We estimated the temperature increase of the crystal lattice due to the laser excitation because we observed some features in the luminescence spectra that could be due to excessive lattice heating. We assumed that all the laser energy absorbed by the sample is transformed instantaneously into phonons. On the basis of simple thermodynamical considerations[23] and using the thermal quantities of GaSe given in Ref. 24, we conclude that the temperature of the samples reaches about 30 K for a laser excitation of 3 MW cm^{-2}. Since the width of the energy gap in GaSe is constant up to a temperature of 30 K,[25] we neglected the lattice heating in our discussion of the experimental results.

IV. EXPERIMENTAL RESULTS AND DISCUSSION

Figure 6 shows a series of photoluminescence (PL) spectra of a T sample of GaSe immersed in superfluid helium and for different excitation intensities. These spectra cover the region from below to above the MT.

Firstly we analyze the region of low J. The emission line at 587.5 nm, labeled ex, is due to the recombination of the direct free exciton.[26] It is well resolved for laser intensities lower than about 200 kW cm^{-2}. The features at longer wavelengths are due to the various scattering processes occurring in a dense exciton gas,[4,5] in which an exciton with a wave vector $K \neq 0$ scatters to $K=0$ through the interaction with another particle (for example an exciton, an electron, or a phonon) before it recombines. As a result of this second-order process, the final energy of the emitted photons is lower than the exciton energy. In particular, the emission labeled ex-e at 589 nm is attributed to the exciton-electron scattering.[5] We found that its integrated luminescence intensity $I_{\text{ex-}e}$ is related to the intensity I_{ex} of the exciton line by

$$I_{\text{ex-}e}(J) \propto I_{\text{ex}}(J)^{1.5} , \quad (28)$$

in agreement with theoretical predictions[27] and with the results of Ref. 5. The broad band which appears about one exciton Rydberg below the ex line (labeled ex-ex in Fig. 6), is structured at the lowest laser intensities.[5,23] This band is due to the overlapping emissions coming from direct as well as indirect exciton-exciton scattering. At low carrier density, the spectral positions of the ex and ex-e are nearly independent of J (see Fig. 8), but a broadening of the exciton line is observed when the carrier density increases.

For increasing J (ranging between 200 and 600 kW cm^{-2}), the integrated exciton luminescence intensity becomes weaker than the ex-e emission which gradually

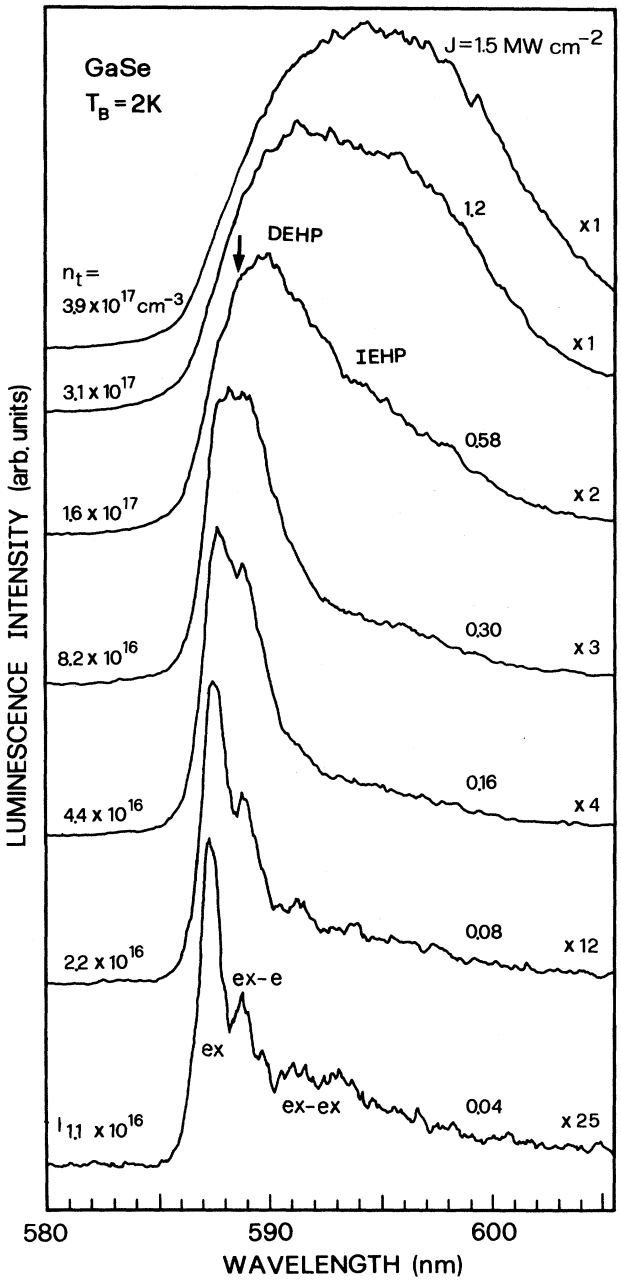

FIG. 6. Series of spontaneous luminescence spectra of a transport grown sample (about 5 μm thick) measured in a superfluid helium bath at a temperature of $T_B=2$ K and photoexcited by a frequency-doubled YAG:Nd laser at 532 nm. The different pump intensities J are indicated on the right side in MW cm^{-2}. The electron-hole pair densities n_t given on the left side have been calculated assuming an e-h recombination time of 0.1 ns (Ref. 22) and an absorption coefficient of 10^3 cm^{-1} (Ref. 21). The relative sensitivity factors for the luminescence intensity are indicated on the extreme right. The labels on the different structures have the following meaning: ex, direct free exciton; ex-e, exciton-electron scattering; ex-ex, exciton-exciton scattering; DEHP, direct electron-hole plasma; and IEHP, indirect electron-hole plasma. An arrow indicates the high-energy shoulder on the DEHP emission which we think is caused by the excitonic enhancement.

dominates the luminescence spectrum. Moreover, the ex line broadens and appears only as a shoulder on the high-energy side of ex-e emission. In this range of laser intensities, the peak of these two lines shifts towards lower energies (see also Fig. 8). Gradually, as the complete ionization of the excitons occurs, the ex-e line is replaced be the wide direct e-h plasma band (DEHP). The emission band due to exciton-exciton scattering diminishes with respect to the other luminescence features and is gradually replaced by the indirect e-h plasma (IEHP) emission. Thus the MT of the excitons in GaSe, as we observe it through our investigation of the e-h recombination in luminescence, is not sharp but smooth and continuous. The continuity of the MT was also observed in direct-gap semiconductors[13,28–31] as well as indirect-gap semiconductors[32–34] where, however, the temperature has to be higher than the critical temperature of the electron-hole liquid.[35] For densities just below the Mott value, the exciton-electron scattering seems to be the main radiative e-h recombination channel in GaSe. The emission connected to exciton-exciton diffusion is never strong.

From our PL spectra we estimate that the MT occurs at about 400 kW cm^{-2}. This corresponds to an e-h pair density $n_t \simeq 1\times10^{17}$ cm^{-3} for the parameters mentioned in Sec. III. This is only a rough experimental estimate of the Mott density n_M because the continuity of the MT makes it difficult to deduce at which pump intensity the transition occurs from the optical spectra without making a numerical analysis. Further, the e-h lifetime is J-dependent and can vary from sample to sample. However, there is a good agreement with the value found in the statically screened approximation (see Fig. 3).

Above 600 kW cm^{-2} we observe a wide and smooth band, which is divided into two humps in some samples. According to the model presented in Ref. 6, it is due to the zero phonon emissions of a direct and indirect electron-hole plasma. With increasing J, these two lines shift to lower energies because of the band-gap reduction. The shoulder (indicated by an arrow in Fig. 6) on the high-energy side of the DEHP could be due to the excitonic enhancement.[12] This shoulder becomes weaker with increasing carrier density and disappears at the highest laser intensities. Effects caused by inhomogeneities in the e-h pair density are improbable since a 5 μm thickness of the sample used for Fig. 6 is lower than the penetration depth (10 μm) of the laser light. Moreover, this shoulder persists for n_t several times higher than n_M, as expected from theory.[8]

Figure 7 shows a series of PL spectra of a Bridgman grown sample of GaSe as a function of the laser intensity. For J lower than 300 kW cm^{-2} the spectra show a main emission line at about 588.0 nm, and a shoulder on the low-energy side at about 589.5 nm, which is the ex-e emission. A similar situation has been described in Ref. 36. At very low intensity ($J \leq 1$ kW cm^{-2}) when the ex-e emission is absent, the ex peak lies at 587.7 nm. Also in transmission the spectra of the B crystals have wider structures than those of the T crystals and they show only a broadened $n=1$ excitonic resonance. Broadening and red shift of the lines might be caused by the cleaving

procedure which could induce faults in the layered structure of the sample.[37] However, the qualitative evolution of the PL spectra of the *B* samples with increasing carrier density is similar to that of the *T* samples. For the sample of Fig. 7, the MT seems to occur at a pump intensity of about 0.8 MW cm^{-2}. Moreover, the high-energy shoulder on the DEHP line caused by *e-h* correlation in the plasma is strongly evident. This shoulder weakens with increasing *J*; for $J=2.9$ MW cm^{-2} it is not visible any more.

We tried to fit these spectra using the random-phase approximation as reported in Ref. 6. We found strong disagreement on the high-energy shoulder marked by an arrow in Fig. 7. This indicates that the neglected excitonic enhancement might be visible in the optical spectra up to quite high *e-h* pair densities. Similar conclusions

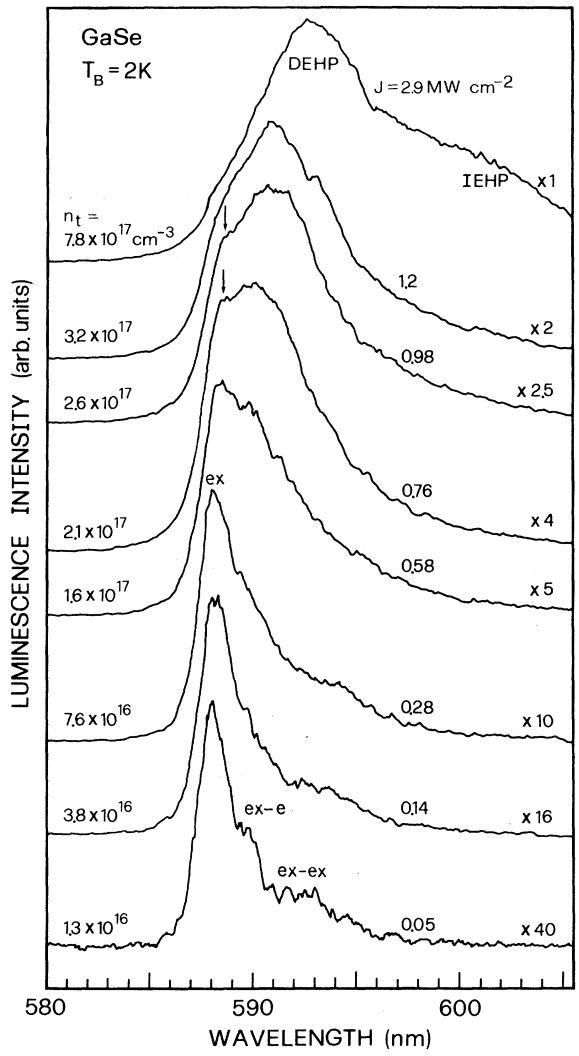

FIG. 7. Series of spontaneous luminescence spectra of a Bridgman grown sample of GaSe ($\sim$4.6 μm thick) measured under the same experimental conditions as described in the caption of Fig. 6. The labels and the numbers have the same meaning as in Fig. 6.

were obtained from luminescence and transmission spectra in direct- and indirect-gap materials.[8,19,34,38,39] At very high excitation intensities in most GaSe crystals the typical two-hump structure appears; only at these highest densities in the spectra can be fitted by a theory which neglects the *e-h* interactions.[6]

In Fig. 8 we show the spectral positions of the ex and ex-*e* lines versus pump intensity *J*, obtained from the *T* crystal of GaSe of Fig. 6. The spectral position of the ex peak remains constant for $J<50$ kW cm^{-2} (i.e., for n_t up to 10^{16} cm^{-3}). At higher densities we observe a red shift of the ex line which amounts to about 2 meV at the MT ($n_M \simeq 10^{17}$ cm^{-3}). We did not observe any increase of the absolute energy of the (fundamental) excitonic level, as has been observed for the 2*s* exciton in GaAs.[13] The results obtained from luminescence experiments agree perfectly with those obtained from two-beam transmission measurements.[20] We compare our experimental results with the theoretically predicted dependence of the exciton energy on the total *e-h* pair density n_t. The curves shown in Fig. 8 have been calculated for "uncorrelated" screening as well as for screening including an exciton contribution (see Sec. II B) and for a carrier temperature of 40 K (in earlier work,[5,6] similar *e-h* pair temperatures have been reported).

There is a good agreement between the computed and

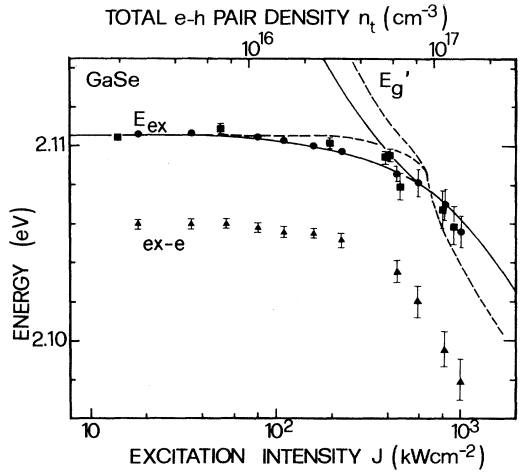

FIG. 8. Spectral position of the peaks in the optical spectra of GaSe (grown by transport reaction) vs excitation intensity. Circles and triangles: luminescence emitted by direct free-exciton recombination (ex) and during an exciton-electron diffusion process (ex-*e*), respectively. At high intensities, the ex-*e* emission is replaced by the direct *e-h* plasma recombination. Squares: excitonic absorption measured in a two-beam transmission experiment (Ref. 20). The error bars are indicated. For comparison, the calculated dependence of the free-exciton energy E_{ex} and the width of the reduced energy gap $E_g'=E_{ex}+E_b$ on the total *e-h* pair density n_t is also shown. The theoretical curves have been shifted horizontally to obtain good agreement with the experimental data. The dashed and solid curves have been calculated as in Figs. 5(b) and 5(c), respectively, but assuming a carrier temperature of 40 K. For the dashed curves, the scale for n_t has to be multiplied by 1.6.

measured exciton energy $E_{ex}(n_t)$, especially in the case of screening including an exciton contribution. At e-h pair densities higher than n_M and in a nondegenerate e-h plasma, the excitonic enhancement has a peak which coincides with the band-gap edge and thus represents somehow the excitonic energy.[8] The spectral position of the shoulder on the high-energy side of the DEHP band which we attribute to the excitonic enhancement compares well with the excitonic energy predicted by Eq. (23) for $n_t > n_M$. We mention, however, that at the Mott density and for a carrier temperature of 40 K the chemical potential $\mu_e + \mu_h$ of the (direct) e-h plasma is only about 4 meV smaller than the width E_g' of the energy gap, therefore, the application of our model which assumes a nondegenerate ensemble of e-h pairs becomes questionable.

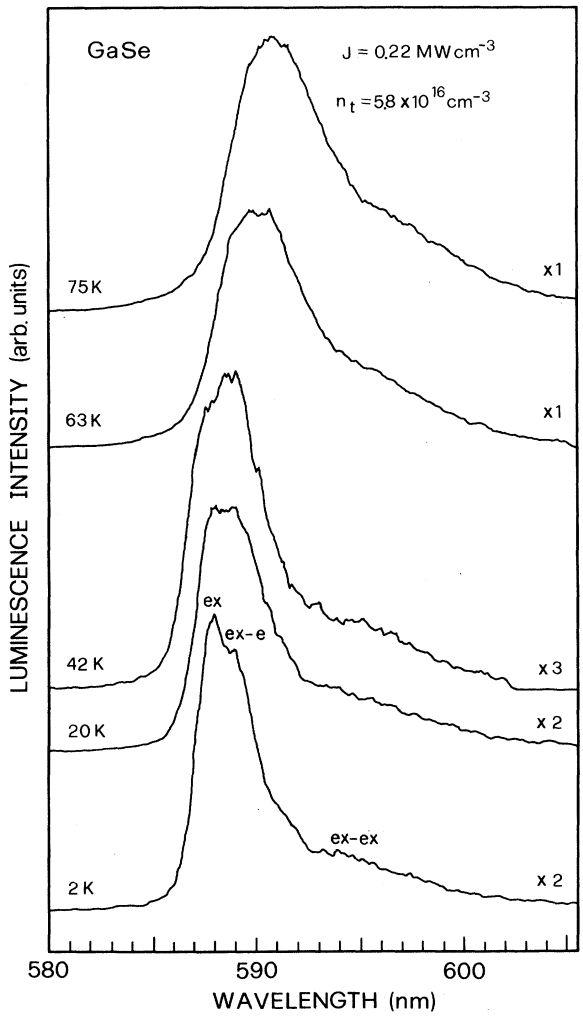

FIG. 9. Series of spontaneous luminescence spectra of a transport grown sample (the same as in Fig. 6) recorded for different temperatures indicated on the left. The sample was excited by a pump intensity of 0.22 MW cm^{-2} which creates an e-h pair density of $\sim 6\times 10^{16}$ cm^{-3}. The symbols used are the same as in Fig. 7.

A red shift of the fundamental exciton energy caused by an increase of the e-h pair density has been observed recently in a few cases, in CdS at low temperatures[28] and in CdSe at 77 K.[29] Transmission and reflectivity measurements in CdS,[30] ZnO,[31] and GaAs (Ref. 13) do not reveal such a red shift. On the theoretical side, simplified[40] as well as more elaborate theories[19,41,42] predict an exciton red shift at least at higher temperatures.

We think that the red shift of the excitonic level we observe in GaSe is not due to crystal lattice heating caused by the laser excitation. Using an excitation intensity of about 200 kW cm^{-2} (at which the ex peak already presents a red shift), we measured the PL spectra for different bath temperatures T_B between 2 and 80 K. As can be seen from Fig. 9, where PL spectra versus temperature at $J = 200$ kW cm^{-2} are shown, the energy position of the ex line remains constant up to $T_B \simeq 40$ K, as is observed at low pump intensities.[25] That is, the lattice temperature does not appreciably rise during the laser pulse, which confirms the theoretical result of Sec. III.

V. CONCLUSION

The presence of dissociated e-h pairs at high densities has two effects: a reduction of the width of the band gap and of the excitonic binding energy. These two effects compensate each other to a large degree and thus the energy of the fundamental exciton remains practically unshifted.[41] More elaborate theories[11,42] predict a small shift of the excitonic level depending on both densities n_{ex} and n_f of bound and dissociated e-h pairs. Our luminescence and absorption spectra of GaSe, measured at different e-h pair densities, reveal a red shift of the excitonic line. This red shift is well accounted for by a first-order theory;[11] we found the densities n_{ex} and n_f from the application of an appropriate mass action law which in turn was based on the exciton binding energies evaluated in static screening approximation. From the red shift of the exciton line we estimate a carrier temperature of about 40 K, which justifies the applicability of our semiclassical model.

Our optical low-temperature study in GaSe confirms earlier theoretical results[10] that the e-h correlation in the e-h fluid in semiconductors is a continuous function of carrier density at the Mott transition, too. These correlations persist in the e-h plasma up to quite high carrier densities and affect the optical spectra through the excitonic enhancement of the radiative interband transition probability. As far as screening is concerned, our analysis seems to indicate that the weakly bound excitons at e-h pair densities not too far below the Mott value cannot be neglected.

ACKNOWLEDGMENTS

We express our thanks to H. Berger for providing the fine GaSe samples. This work was supported in part by the Italian "Consiglio Nazionale delle Ricerche" (Contract No. 85.00355.02) and by the "Fonds National Suisse de la Recherche Scientifique."

APPENDIX

Simple expressions for the different contributions to the excitonic shift ΔE_{ex} [Eq. (23)] as a function of temperature T_e and mass ratio σ have been derived by Röpke *et al.*[11] They give general formulas for δ_f^1 and δ_{ex}; for δ_f^2 and δ_f^3, they consider only the special case of equal electron and hole masses. We thus calculated δ_f^2 and δ_f^3 numerically for arbitrary values of σ, and we proceeded as follows.

We start from Eq. (2.19) of Ref. 11:

$$\Delta E_{ex}=-\sum_{npqq'} V(\mathbf{q}')\psi_1(\mathbf{p})\psi_1(\mathbf{p}+\mathbf{q})\frac{\omega_{pl}^2}{2\omega_{q'}}\left[\frac{g(\hbar\omega_{q'})-g_{eh}(E_{nq'})}{E_{10}+\hbar\omega_{q'}-E_{nq'}}+\frac{1+g(\hbar\omega_{q'})+g_{eh}(E_{nq'})}{E_{10}-\hbar\omega_{q'}-E_{nq'}}\right]$$
$$\times\left[\psi_n\left[\mathbf{p}+\frac{m_e}{M}\mathbf{q}'\right]-\psi_n\left[\mathbf{p}-\frac{m_h}{M}\mathbf{q}'\right]\right]\left[\psi_n\left[\mathbf{p}+\mathbf{q}+\frac{m_e}{M}\mathbf{q}'\right]-\psi_n\left[\mathbf{p}+\mathbf{q}-\frac{m_h}{M}\mathbf{q}'\right]\right], \tag{A1}$$

where $V(\mathbf{q})$ is the Fourier transform of the Coulomb potential, $\psi_n(\mathbf{q})$ is the wave function of an exciton state with principal quantum number n, E_{nq} is the total energy of an e-h pair with momentum $\mathbf{q}$ and principal quantum number n, $\omega_{pl}=\omega_{q=0}$ is the plasma frequency, $\hbar\omega_q$ is the plasmon energy in plasmon pole approximation, $g(\hbar\omega_q)$ is the plasmon distribution function, $g_{eh}(E_{nq})$ is the e-h pair distribution function, m_e is the electron mass, m_h is the hole mass, $M=m_e+m_h$ is the translational exciton mass, $\mathbf{p},\mathbf{q},\mathbf{q}'$ are momenta, and the sum is over the whole exciton energy spectrum.

As far as δ_f^2 is concerned, which describes the plasmon stimulated transitions from the excitonic ground state into a bound two-particle state, we consider only the $n=2$ terms in the sum. Further, introducing the Fourier transform of the exciton wave functions,[43] the integral in Eq. (A1) can be evaluated in a straightforward way,[23] obtaining

$$\delta_f^2=-2^8\int_0^\infty dx\frac{1}{\omega(x)}\left[\frac{g(\omega(x))}{\epsilon_+}+\frac{1+g(\omega(x))}{\epsilon_-}\right]\left[\frac{6.75-(bx)^2}{[2.25+(bx)^2]^3}-\frac{6.75-(cx)^2}{[2.25+(cx)^2]^3}\right]$$
$$+2^89\int_0^\infty dx\frac{1}{\omega(x)}\left[\frac{g(\omega(x))}{\epsilon_+}+\frac{1+g(\omega(x))}{\epsilon_-}\right]\left[\frac{bx}{[2.25+(bx)^2]^3}+\frac{cx}{[2.25+(cx)^2]^3}\right] \tag{A2}$$

where we introduced the following definitions: $a\equiv(1-\sigma)/(1+\sigma)$, $b\equiv(\sigma)/(1+\sigma)$, $c\equiv1/(1+\sigma)$, and $T^*\equiv k_BT_e/E_B$; furthermore,

$$\omega(x)\equiv\left[x^2\left[T^*+\frac{x^2}{4}\right]\right]^{1/2}, \tag{A3}$$

$$g(\omega)\equiv\left[1-\exp\frac{\omega}{T^*}\right]^{-1}, \tag{A4}$$

and

$$\epsilon_\pm(\omega,x)\equiv\pm\omega(x)-bcx^2-0.75\ . \tag{A5}$$

To calculate δ_f^3, which describes the plasmon stimulated transition from the ground state into scattering two-particle states, we have to consider the properties of a free e-h pair.

(i) The e-h energy can be split in a contribution coming from the relative motion and another from the center-of-mass motion:

$$E_{n\mathbf{P}}=\frac{\hbar^2P^2}{2M}+\frac{\hbar^2k^2}{2m_{eh}}+E_g\ , \tag{A6}$$

where m_{eh} is the exciton reduced mass and $\mathbf{P}$ the momentum of the center-of-mass.

(ii) The wave function for the relative motion of the interacting e-h pair is given by a plane wave in the first Born approximation,[11] i.e.,

$$\Psi_{\mathbf{P}}(\mathbf{k})\simeq\psi_{\tilde{\mathbf{k}}}(\mathbf{k})\simeq\delta_{\tilde{\mathbf{k}}}(\mathbf{k}) \tag{A7}$$

and it describes a free pair in the $\tilde{\mathbf{k}}$ state composed by an electron with wave vector $\mathbf{k}_e=-\mathbf{k}+(m_e/M)\mathbf{P}$ and a hole with $\mathbf{k}_h=\mathbf{k}+(m_h/M)\mathbf{P}$. With these assumptions and considering only final states in the continuum, Eq. (A1) becomes

$$\Delta E_{\rm ex}^{\infty}=-\sum_{\mathbf{kpqq'}} V(\mathbf{q'})\psi_1(\mathbf{p})\psi_1(\mathbf{p}+\mathbf{q})\frac{\omega_{\rm pl}^2}{2\omega_{\mathbf{q'}}}\left[\frac{g(\hbar\omega_{\mathbf{q'}})-g_{eh}(E_{\mathbf{kq'}})}{E_{10}+\hbar\omega_{\mathbf{q'}}-E_{\mathbf{kq'}}}+\frac{1+g(\hbar\omega_{\mathbf{q'}})+g_{eh}(E_{\mathbf{kq'}})}{E_{10}-\hbar\omega_{\mathbf{q'}}-E_{\mathbf{kq'}}}\right]$$
$$\times\left[\delta_{\mathbf{k}}\left[\mathbf{p}+\frac{m_e}{M}\mathbf{q'}\right]-\delta_{\mathbf{k}}\left[\mathbf{p}-\frac{m_h}{M}\mathbf{q'}\right]\right]\left[\delta_{\mathbf{k}}\left[\mathbf{p}+\mathbf{q}+\frac{m_e}{M}\mathbf{q'}\right]-\delta_{\mathbf{k}}\left[\mathbf{p}+\mathbf{q}-\frac{m_h}{M}\mathbf{q'}\right]\right] \tag{A8}$$

Then, we sum over $\mathbf{p}$ and $\mathbf{q}$ using the properties of δ and we neglect $g_{eh}(E_{\mathbf{kq'}})$ because it is a higher-order term in the density:

$$\Delta E_{\rm ex}^{\infty}=-\sum_{\mathbf{q'}}\int_{-\infty}^{+\infty}d\omega\, V(\mathbf{q'})\frac{\omega_{\rm pl}^2}{2\omega_{\mathbf{q'}}}\left[\frac{g(\hbar\omega_{\mathbf{q'}})}{\hbar\omega_{\mathbf{q'}}-\hbar\omega}+\frac{1+g(\hbar\omega_{\mathbf{q'}})}{-\hbar\omega_{\mathbf{q'}}-\hbar\omega}\right]G(\mathbf{q'},\omega)\ , \tag{A9}$$

where

$$G(\mathbf{q},\omega)=\sum_{\mathbf{k}}\left[\psi_1\left[\mathbf{k}-\frac{m_e}{M}\mathbf{q}\right]-\psi_1\left[\mathbf{k}+\frac{m_h}{M}\mathbf{q}\right]\right]^2\delta\left[\frac{\hbar^2}{2m_e}\left[\mathbf{k}-\frac{m_e}{M}\mathbf{q}\right]^2+\frac{\hbar^2}{2m_h}\left[\mathbf{k}+\frac{m_h}{M}\mathbf{q}\right]^2+E_{10}-\hbar\omega\right]\ . \tag{A10}$$

To compute $G(\mathbf{q},\omega)$ we introduce the wave function in $\mathbf{k}$ space:[43]

$$\psi_1(\mathbf{k})=\sqrt{64\pi}(1+k^2)^{-2} \tag{A11}$$

and the bipolar coordinates $p_1=|\mathbf{k}+(m_e/M)\mathbf{q}|$, $p_2=|\mathbf{k}-(m_h/M)\mathbf{q}|$, and ϕ. With the transformation

$$\begin{aligned} y&=\tfrac{1}{2}(p_1^2+p_2^2+2)\ ,\\ z&=p_2^2-p_1^2\ , \end{aligned} \tag{A12}$$

we obtain

$$G(q,\omega)=\frac{32}{q^2}\int_0^{2\pi}d\phi\int\int_{\mathcal{D}}dy\,dz\frac{[(y-z/2)^2-(y+z/2)^2]^4}{(y-z/2)^4(y+z/2)^4}\delta\left[\frac{(y+z/2)+(y-z/2)\sigma}{1+\sigma}-\omega\right]\ , \tag{A13}$$

where $\mathcal{D}$ is the set of points on the surface defined by

$$4q^2y=z^2+4q^2+q^4\ . \tag{A14}$$

Using a computer program called MACSYMA[44] which is able to perform algebraic computation, we finally got $G(q,\omega)$ and thus δ_f^3:

$$\delta_f^3=-\frac{2^{12}}{\pi}\int_0^{\infty}dx\int_{y_{\rm min}}^{\infty}dy\frac{1}{x(y+1)^3\omega(x)}\left[\frac{g(\omega(x))}{\omega(x)-y}+\frac{1+g(\omega(x))}{\omega(x)+y}\right][F(y_2)-F(y_1)]\ , \tag{A15}$$

where

$$y_{\rm min}=1+bcx^2\ , \tag{A16}$$

$$F(y)=\frac{1}{(1-y^2)^3}\left[\frac{a^2-1}{16}(y^5-y)+\frac{a^2+1}{16}y^3+\frac{a}{2}y^2-\frac{a}{6}\right]+\frac{a^2-1}{32}\ln\left|\frac{y+1}{y-1}\right|\ , \tag{A17}$$

$$y_1=\frac{-ax^2-2x(y-y_{\rm min})^{1/2}}{2y+a^2x^2+2a^2x(y-y_{\rm min})^{1/2}}\ , \tag{A18}$$

$$y_2=\frac{-ax^2+2x(y-y_{\rm min})^{1/2}}{2y+a^2x^2-2a^2x(y-y_{\rm min})^{1/2}}\ . \tag{A19}$$

In order to get the curves shown in Fig. 4, the integrals in formulas (A2) and (A15) have been evaluated numerically.

*Present address: Institut de Micro- et Optoélectronique, Ecole Polytechnique Fédérale, PH-Ecublens, CH-1015 Lausanne, Switzerland.

[1]W. Ebeling, W. D. Kraeft, and D. Kremp, *Theory of Bound States and Ionization Equilibrium in Plasmas and Solids,* Vol. 5 of *Ergebenisse der Plasmaphysik und Gaselektronik* (Akademie-Verlag, Berlin, 1976).

[2]F. J. Rogers, H. C. Graboske, Jr., and D. J. Harwood, Phys. Rev. A **1**, 1576 (1970); F. J. Rogers, *ibid.* **4**, 1145 (1971).

[3]H. Haug and S. Schmitt-Rink, Prog. Quantum Electron. **9**, 3 (1984).

[4]A. Mercier and J. P. Voitchovsky, Phys. Rev. B **11**, 2243 (1975).

[5]V. Capozzi and J. L. Staehli, Phys. Rev. B **28**, 4461 (1983).

[6]J. L. Staehli and V. Capozzi, Helv. Phys. Acta **58**, 262 (1985).

[7]G. D. Mahan, Phys. Rev. **153**, 882 (1967).

[8]L. Pavesi, J. L. Staehli, and V. Capozzi, J. Phys. C **21**, 1485 (1988).
[9]R. Zimmermann, Phys. Status Solidi B **86**, K63 (1978).
[10]H. Stolz and R. Zimmermann, Phys. Status Solidi B **94**, 135 (1979); R. Zimmermann, and H. Stolz, *ibid.* **131**, 151 (1985).
[11]G. Röpke, T. Seifert, H. Stolz, and R. Zimmermann, Phys. Status Solidi B **100**, 215 (1980).
[12]L. Pavesi, J. L. Staehli, and V. Capozzi, Solid State Commun. **61**, 321 (1987).
[13]G. W. Fehrenbach, W. Schäfer, and R. G. Ulbrich, J. Lumin. **30**, 154 (1985).
[14]L. D. Landau and E. M. Lifshitz, *Statistical Physics* (Pergamon, Oxford, 1970), Sec. 77.
[15]R. G. Newton, *Scattering Theory of Waves and Particles* (McGraw-Hill, New York, 1966).
[16]J. Collet, J. Phys. Chem. Solids **46**, 417 (1985).
[17]From earlier work on the three component plasma in GaSe (Ref. 6) we deduce that the density of M electrons is at the most of the same magnitude as that of Γ electrons.
[18]F. Thuselt, Phys. Lett. **94A**, 93 (1983).
[19]H. Schweizer *et al.*, Phys. Rev. Lett. **51**, 698 (1980).
[20]L. Pavesi, V. Capozzi, and J. L. Staehli, Phys. Scr. **38**, 627 (1988).
[21]R. Le Toullec, N. Piccioli, and J. C. Chervin, Phys. Rev. B **22**, 6162 (1980); R. Le Toullec *et al.*, Nuovo Cimento **38B**, 159 (1977).
[22]T. Kushida *et al.*, Nuovo Cimento **39B**, 650 (1977); J. Collet, private communication.
[23]L. Pavesi, Tesi di Laurea, Universita' di Trento (1985).
[24]*Numerical Data and Functional Relationships in Science and Technology, New Series,* Vol. 17 of *Landolt-Börnstein,* edited by O. Madelung (Springer-Verlag, Berlin, 1983).
[25]J. P. Voitchovsky and A. Mercier, Nuovo Cimento **22B**, 273 (1974).
[26]A. Mercier, E. Mooser, and J. P. Voitchovsky, Phys. Rev. B **12**, 4307 (1975).
[27]C. Benoit à La Guillame, J. Debever, and F. Salvan, Phys. Rev. **177**, 567 (1969).
[28]K. Kempf, G. Schmieder, G. Kurtze, and C. Klingshirn, Phys. Status Solidi B **107**, 297 (1981).
[29]A. W. Mol, R. A. Muribeca, and E. A. Meneses, Solid State Commun. **53**, 111 (1985).
[30]V. G. Lysenko and V. I. Revenko, Fiz. Tverd. Tela **20**, 2144 (1978) [Sov. Phys.—Solid State **20**, 1238 (1978)].
[31]K. Bohnert *et al.*, Phys. Status Solidi B **98**, 175 (1980).
[32]L. Smith and J. P. Wolfe, Phys. Rev. Lett. **57**, 2314 (1986).
[33]F. M. Steranka and J. P. Wolfe, Phys. Rev. B **34**, 1014 (1986).
[34]I. Balslev, J. Lumin. **30**, 162 (1985).
[35]The e-h droplet formation in indirect-gap semiconductors below the critical temperature occurs by nucleation at densities which can be much lower than the Mott value; see, e.g., R. M. Westervelt, J. L. Staehli, and E. E. Haller, Phys. Status Solidi B **90**, 557 (1978).
[36]T. Ugumori, K. Masua, and S. Namba, J. Phys. Soc. Jpn. **41**, 1991 (1976).
[37]V. Capozzi and K. Maschke, Phys. Rev. B **34**, 3924 (1986).
[38]M. Guzzi, J.L. Staehli, M. Capizzi, and R. A. Logan, Europhys. Lett. **2**, 547 (1986).
[39]L. Bànyai and S. W. Koch, Z. Phys. B **63**, 283 (1986).
[40]I. Balslev and A. Stahl, Solid State Commun. **59**, 371 (1986).
[41]R. Zimmermann *et al.*, Phys. Status Solidi B **90**, 175 (1978).
[42]F. Boldt, K. Henneberger and V. May, Phys. Status Solidi B **130**, 675 (1985).
[43]S. Flügge, *Practical Quantum Mechanics* (Springer-Verlag, Berlin, 1974).
[44]Project MAC's SYmbolic MAnipulation System (MACSYMA), Mathlab Group, MIT Laboratory for the Computer Science, Cambridge (1983).
[45]G. Ottaviani *et al.*, Solid State Commun. **14**, 933 (1974).